Journal of Marine Research, 47, 169–196, 1989

Rates of vertical mixing, gas exchange and new production: Estimates from seasonal gas cycles in the upper ocean near Bermuda

by William S. Spitzer[1] and William J. Jenkins[1]

ABSTRACT

Argon measurements, obtained from one year of monthly detailed vertical profiles near Bermuda (32N 64W), show a maximum in argon supersaturation of about 4% in the seasonal thermocline in late summer. Since the argon supersaturation is 3–4 times smaller than that of oxygen, most of the oxygen supersaturation is not of physical origin and hence must result from biological production.

In the winter mixed layer, air injection produces argon supersaturation in spite of high gas exchange rates. During spring and summer, radiative heating, air injection, and an upward argon flux create an even larger supersaturation in the mixed layer. In the seasonal thermocline, radiative heating maintains argon concentrations above solubility equilibrium in spite of vertical mixing.

The observed seasonal cycles of temperature, argon, helium, and oxygen are simulated with an upper ocean model. We linearized the model's response to variations in vertical diffusivity, air injection, gas exchange rate, and new production and then used an inverse technique (singular value decomposition) to determine the values of these parameters that best fit the data. A vertical turbulent diffusivity of $0.9 \pm 0.1 \times 10^{-4}$ m^2 s^{-1} is consistent with both the thermal history and subsurface argon distribution. The rate of air injection, determined to ±25%, is similar to previous estimates. The seasonally-averaged gas exchange rate is 17 ± 12% lower than predicted by Liss and Merlivat (1986). We estimate a lower limit to depth-integrated new production below the mixed layer of 4.3 ± 1.7 moles O_2 m^{-2} yr^{-1} during 1985, and obtain an estimate of 5.6 ± 1.5 moles O_2 m^{-2} yr^{-1} if new production in the mixed layer is fixed at zero.

1. Introduction

The development of a summer oxygen maximum in the seasonal thermocline is a common feature of subtropical waters (Schulenberger and Reid, 1981), and has been attributed to "new" photosynthetic production (*op cit;* Jenkins and Goldman, 1985). However, physical processes such as radiative heating and air injection may produce supersaturation unrelated to biological activity. On the other hand, much of the biogenic oxygen may be lost from the seasonal thermocline via vertical mixing and gas exchange. Measurements of dissolved argon can quantify these effects since argon is an

1. Department of Chemistry, Woods Hole Oceanographic Institution, Woods Hole, Massachusetts, 02543, U.S.A.

inert gas whose physical properties (e.g. solubility and diffusivity) are close to those of oxygen and have a similar temperature dependence (Benson, 1965). In the summer of 1985, Craig and Hayward (1987) compared oxygen and argon supersaturations at two stations in the subtropical North Pacific, and concluded that most of the excess oxygen was photosynthetically produced since argon was much less supersaturated than oxygen.

Since the solubility of argon has a strong temperature dependence, seasonal heating forces an annual cycle in argon concentration. Argon's inability to "keep up" with the thermal cycle, as measured by its departures from solubility equilibrium, can be used to estimate rates of transport processes in the upper ocean. We will couple measurements of the seasonal cycles of argon, helium, temperature, and oxygen with an upper ocean model (Chou, 1985; Musgrave *et al.*, 1988). By linearizing the model's response to parameter variations and then applying an inverse technique (singular value decomposition), we then infer rates of vertical mixing, gas exchange, air injection, and new production.

2. Methods

The results reported here are from the first year (April 1985—April 1986) of a three-year study at Station S (32N 64W), situated 25 km southeast of Bermuda in the Sargasso Sea. We have augmented an ongoing series of biweekly hydrographic stations which measure temperature, salinity and oxygen at standard depths with approximately monthly sampling for nutrients, argon, helium, and tritium and an additional shallow cast to obtain approximately 10 m resolution in the upper 100 m.

Samples for argon analysis are collected by gravity-feed from Niskin bottles and stored in copper tubes containing 13 grams of seawater (Weiss, 1968; Jenkins and Clarke, 1976). In the laboratory, the seawater is quantitatively degassed under vacuum, purified to remove contaminant gases, and the argon is then measured by isotope dilution mass spectrometry. Concentrations are measured as (cc at S.T.P.) $(\text{g seawater})^{-1}$. Saturation anomalies (ΔAr) are expressed as percent deviations from smoothed gas solubilities compiled by Weiss (1970; 1971a), which have a precision of about 0.2%.

Replicate analyses of Vineyard Sound, MA surface water obtained by bucket sampling indicate that the total uncertainty associated with copper tube sampling, storage, extraction and mass spectrometric analysis is 0.3%. Absolute calibrations of the isotopic standards, volumes and temperatures are accurate to 0.15% and traceable to National Bureau of Standards (N.B.S.). A series of 12 samples from a depth of 2000 $\pm$ 200 m show no statistically significant trends with a mean ΔAr of -0.7%, but have a somewhat larger sample standard deviation of 0.6%. This is an upper bound to the analytical error because it includes any natural variations (presumed to be small at this depth), but may indicate an additional source of error. Laboratory experiments suggest that if the seawater warms up during sample collection, exsolved bubbles may

occasionally be trapped in the samplers. Extreme conditions created in the laboratory resulted in a 2–3% supersaturation, but more typical conditions yielded 0.3–0.5%. Recent measurements indicate that this problem can be minimized with careful sampling. In total, however, the analytical error is small compared to the seasonal range of argon concentrations (about 15%).

Helium samples are collected in copper tube samplers containing 45 grams of seawater, and the total helium content is measured by peak height manometry to a precision of 0.2% (Lott and Jenkins, 1984). Concentrations are measured as (cc at S.T.P.) (g seawater)$^{-1}$. Saturation anomalies (ΔHe) are expressed as percent deviations from smoothed gas solubilities compiled by Weiss (1971b), which have a precision of 0.3%.

Since the seasonal cycle of oxygen will be used to infer rates of new production, the analytical error in the oxygen measurements must also be assessed. Oxygen is determined by modified Winkler titration (Carritt and Carpenter, 1966) at the Bermuda Biological Station (B.B.S.). Jenkins and Goldman (1985) estimated an upper bound to the analytic error in the B.B.S. oxygen analyses from the reproducibility of deep water concentrations; during 1961–1978 the sample standard deviation at 2000 m was 0.125 ml l^{-1}, with no statistically significant seasonal or long-term trends. During 1985, the reproducibility at this depth is comparable ($\pm$0.15 ml l^{-1}) and similar estimates were obtained by comparing duplicate analyses ($\pm$0.17 ml l^{-1}) and by computing the scatter about a mean climatological oxygen vs. temperature curve ($\pm$0.19 ml l^{-1} for 3°C $< T <$ 16°C) for the 1985 measurements. In 1985, the mean value at 2000 m was 6.12 ml l^{-1}, just slightly higher (by 0.06 ml l^{-1}) than the 1961–1978 mean.[2]

3. Results

The time series measurements are presented in Figure 1 and in the Appendix. The seasonal cycle of temperature at Bermuda (Fig. 1a) is characterized by deep convection in the late winter, followed by increasing stratification during spring and summer, and finally erosion of the seasonal thermocline in the fall. The seasonal cycle of argon concentration (Fig. 1b) is qualitatively similar to that of temperature, since the argon cycle is controlled by the strong temperature dependence of argon solubility.

By comparing the observed argon concentrations to those expected from solubility equilibrium, thermal effects can be separated from other physical processes. The seasonal cycle in percent argon supersaturation in the upper 200 m is shown in Figure 1c, with the mixed layer history presented in more detail in Figure 2a. In late winter,

2. Deep oxygen analyses from January–February, 1986 were systematically higher by 0.4–0.6 ml l^{-1} than the climatological mean, whereas a nearby Oceanus cruise (P. Brewer, pers. comm.) did not reveal such anomalies. We attribute the anomalies to analytical problems, and hence these oxygen data have not been included in the analysis.

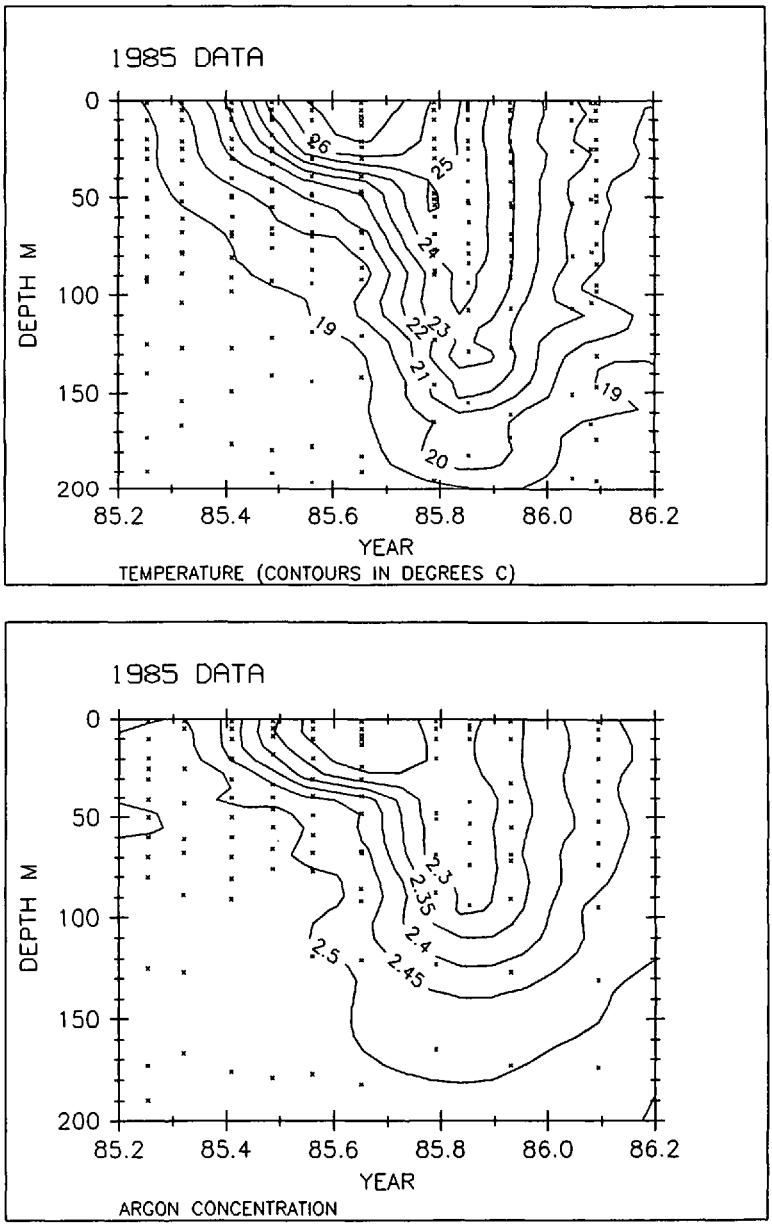

Figure 1. Seasonal distributions for April 1985–April 1986 of: (a) temperature (°C), (b) argon concentration (10^{-4} cc g^{-1}), (c) ΔAr (percent supersaturation), and (d) ΔO_2 (percent supersaturation). Sample locations are indicated by crosses. Year-time is computed as the fraction of the year elapsed since January 1 (e.g. 85.50 is equivalent to July 1, 1985). The argon distribution is driven by seasonal heating, as seen from the similarity to the thermal cycle. Oxygen is controlled only partly by physical processes, hence the amplitude of its seasonal cycle is larger than that of argon.

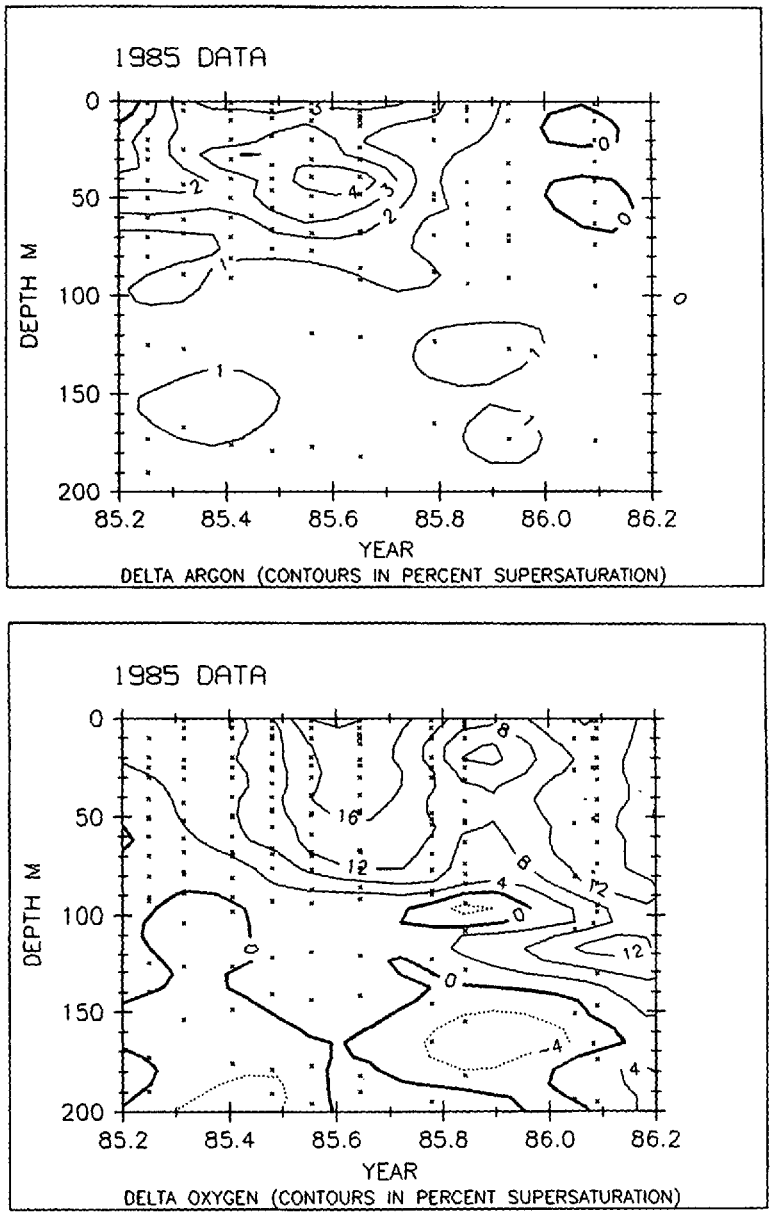

Figure 1. (Continued)

argon supersaturation in the deep mixed layer reflects a dynamic balance between air injection and gas exchange. In spring and summer, the mixed layer supersaturation increases because outgassing can remove only a fraction of the supersaturation produced by radiative heating, air injection, and the flux of argon from below. In the seasonal thermocline, radiative heating sustains a subsurface maximum in argon

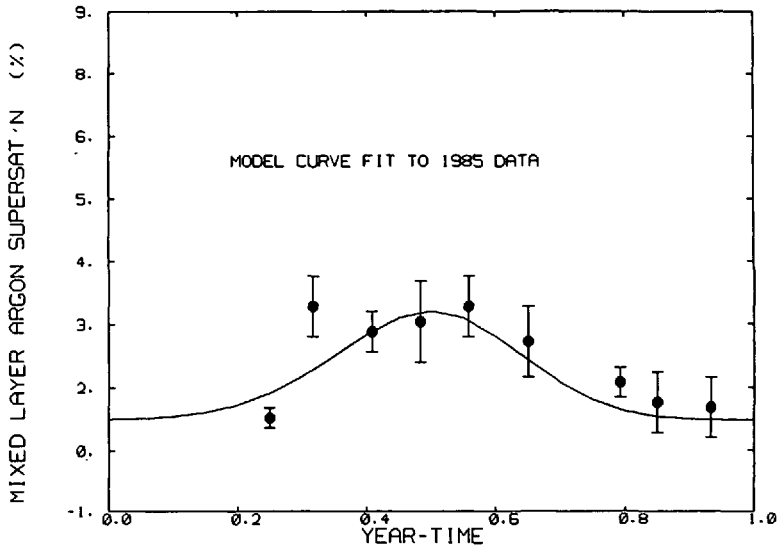

ARGON

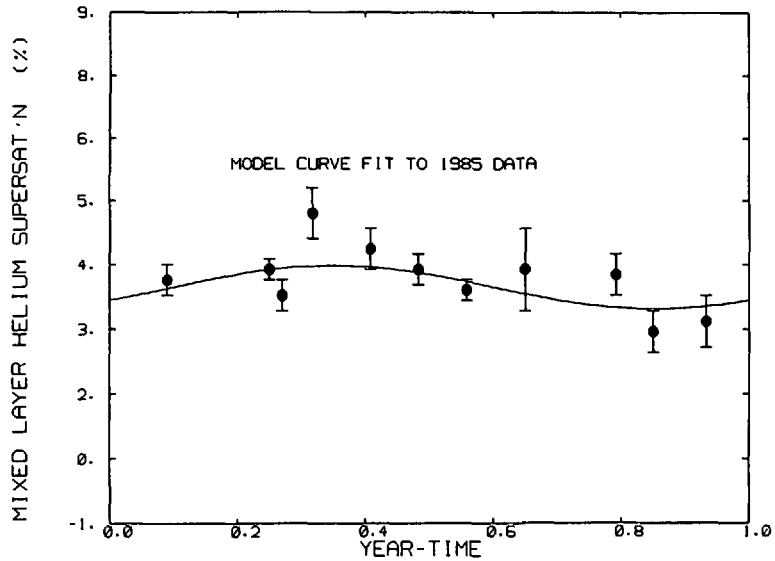

HELIUM

Figure 2. Seasonal cycle of supersaturation of (a) argon and (b) helium, where each data point represents an average of several samples within the mixed layer (mixed layer depth determined using a $\Delta T = 0.5°C$ criterion) and the error bars are statistical uncertainties associated with the mean value. Solid lines are model fits using nonlinear least-squares (see text for details). The argon cycle differs from that of helium because it is driven mostly by radiative heating rather than air injection.

supersaturation despite vertical mixing. In the fall, cooling and convective mixing erode the subsurface maximum and gas exchange erases the remnant supersaturation in the mixed layer. Rapid gas exchange and air injection "recharge" argon concentrations to their winter-time values.

The seasonal cycle of percent oxygen supersaturation (Fig. 1d) is qualitatively similar to that of argon down to the base of the euphotic zone, below which respiration produces oxygen undersaturation. However, the seasonal amplitude is much larger because oxygen is biologically produced *in situ,* whereas the argon cycle is driven solely by physical processes. The seasonal cycle of oxygen at Bermuda, discussed by Jenkins and Goldman (1985), is characterized by near saturation values in the deep winter mixed layer with some slight undersaturation due to rapid cooling and the upward mixing of oxygen-depleted water from below. During spring and summer, a subsurface oxygen maximum develops in the seasonal thermocline, accompanied by a "counterpoint" pattern of undersaturation below due to respiration. Finally, fall cooling and convective mixing lead to erasure of the subsurface extrema.

4. A seasonal upper ocean model

Our understanding of the gas cycles can be refined using a seasonal upper ocean model. The model's success in predicting the argon distribution would provide a good test of its simulation of physical processes affecting oxygen, a necessary prerequisite for inferring biological oxygen production. We use an adaptation of the model presented by Price *et al.* (1986), which has succeeded in simulating the seasonal temperature cycle for climatological (1960–1970 average) conditions at Station S (Chou, 1985), and is similar to the model used by Musgrave *et al.* (1988). This one-dimensional vertical model contains a bulk mixed layer, whose depth is determined from static stability, bulk Richardson number, and gradient Richardson number criteria. The only "tunable" parameter is a vertical turbulent diffusivity, required to transport heat and tracers below the mixed layer. A diffusivity (κ) of $\sim 1 \times 10^{-4}$ m^2 s^{-1} best matches the climatological mean temperature cycle, and was varied between $0.7–1.7 \times 10^{-4}$ m^2 s^{-1} in model runs. The model is forced by seasonally-modulated climatological values for heat flux (Bunker, 1975), Ekman pumping (Leetmaa and Bunker, 1978), and radiative heating (Bunker, 1975) with a Jerlov type IA absorption curve (Paulson and Simpson, 1977). We used Bunker's climatological monthly-averaged winds from Marsden Square 115, interpolated to a 1° × 1° grid (Isemer and Hasse, 1985). Land-based records from the Bermuda Naval Air Station suggest that the monthly averaged winds in 1985 were similar to the climatological values. We have simulated shorter period wind variations by adding a 4-day sinusoidal component (Chou, 1985). A stochastic wind parameterization used by Musgrave *et al.* (1988) gives similar results.

Gas exchange rates are computed as a function of wind speed using the relationship proposed by Liss and Merlivat (1986), with a $-\frac{1}{2}$ power dependence on the Schmidt

number (ratio of kinematic viscosity to molecular diffusivity). Regression statistics suggest an uncertainty of about ±15% over the domain of interest. In model runs, the gas exchange rate is varied between 0.5 and 2.0 times the Liss and Merlivat formulation ($g = 0.5 - 2.0$).

Air injection is simulated by bubble processes with a power law dependence on wind speed. The total air injection flux for each gas is parameterized as:

$$\text{Flux}_i = (\alpha_i)(a_{\text{inj}})(f_t + \Gamma f_p)(6 \times 10^{-8}\ \text{cc m}^{-2}\ \text{s}^{-1})\{u_{10}/(10\ \text{m s}^{-1})\}^{\gamma}$$

where the flux is measured in (cc @ S.T.P.) $\text{m}^{-2}\,\text{s}^{-1}$, α_i is the mole fraction of the gas in air, and u_{10} is the wind speed at 10 m above the sea surface (m s^{-1}). Two modes of bubble trapping (total and partial trapping) are used (Jenkins, 1988), with f_t and f_p as the relative fractions of each component constrained by $f_t + f_p = 1$. The air injection flux is normalized to that for helium at 20°C by using a normalization factor (Γ) associated with the diffusive limitation for gas transfer from the bubbles given by:

$$\Gamma = (D_i/D_o)^{2/3}$$

where D_o is the molecular diffusivity of helium at 20°C. In model runs, the air injection amplitude (a_{inj}) was varied from 0.0–1.0, the wind speed exponent (γ) was varied from 1.0–3.5, and the fraction of total trapping (f_t) was varied between 0.0–1.0.

New production is implemented using two regions of oxygen production, one in the seasonal thermocline and the other near the surface. In the seasonal thermocline, the depth distribution of new production is represented as a truncated sine curve ($0 \leq \Theta \leq \pi$) between 25 and 75 m with a maximum at 50 m. Although the true depth dependence is unknown, this parameterization tends to give a conservative estimate of the required oxygen production (Chou, 1985; Musgrave *et al.*, 1988). Near-surface production is specified as a constant value in the upper 5 m, which is then distributed throughout the mixed layer. Both production terms are seasonally modulated with a maximum in production in early spring (Chou, 1985; Musgrave *et al.*, 1988). The annual oxygen production in the seasonal thermocline (P_{50}) and in the mixed layer (P_{ml}) were each varied between 0–10 moles $\text{m}^{-2}\ \text{yr}^{-1}$. Below 100 m, the depth-integrated respiration balances the total production above. The consumption rate is assumed to decrease linearly with depth to 300 m (the maximum depth in the model), which approximates measurements of oxygen utilization rates (Jenkins, 1987).

5. Linearization of model response

The features associated with the seasonal cycles in temperature, argon, and oxygen are dependent on several physical (and for oxygen, biological) processes. Results from a sample model run (Fig. 3) demonstrate that the model simulates these features qualitatively, but the quantitative agreement depends on the precise choice of model parameters. We ran the model over a range of parameters for each process (vertical

mixing, gas exchange, air injection, and productivity), and then linearized the model responses in terms of "indices" that could be calculated from the data. These indices were selected as well-defined diagnostics of the processes controlling the tracer distributions. The functional forms of these equations were chosen empirically to best match the model responses. Uncertainties cited with each diagnostic equation (see also Table 1) represent the error associated with linearizing the model response over the parameter range explored. We then used an inverse technique (singular value decomposition) to calculate the set of model parameters that best fit the data.

a. Vertical mixing. Since seasonal heating drives the argon cycle, it is critical to accurately represent the thermal cycle. The only adjustable model parameter which affects temperature is the vertical diffusivity. If vertical mixing is too weak, too much heat is trapped near the surface; if it is too strong, too much heat is transferred below the mixed layer. The strongest constraint on the diffusivity is the mixed layer temperature difference between winter and summer (Fig. 4), for which we obtain:

$$\Delta T_{ml}[s - w] = 6.31 + 2.47(10^{-4}/\kappa) \pm 0.2°\text{C} \quad (1)$$

where the diffusivity κ is measured in $m^2\ s^{-1}$. The degree to which the subsurface argon concentration lags behind the *in situ* temperature increase between winter and summer is also sensitive to vertical exchange in the seasonal thermocline. In the absence of vertical exchange, the observed seasonal warming at a depth of 50 m would produce an argon supersaturation of 8%. Since the observed supersaturation is much smaller, the removal of argon by vertical transport (and subsequent gas exchange) is significant.

The model predicts that the maximum argon supersaturation in the summer thermocline ($\Delta Ar_{max}[s]$) is affected not only by the vertical diffusivity (κ), but also by the gas exchange rate (g), air injection amplitude (a_{inj}) and trapping mode fraction (f_t):

$$\Delta Ar_{max}[s] = 0.76(10^{-4}/\kappa) + 2.2(1/g) + 1.7(a_{inj})(0.3f_t + 0.9) \pm 0.1\% \quad (2)$$

As the gas exchange rate is reduced, more argon is trapped in the mixed layer and hence the flux from the seasonal thermocline is also reduced. As vertical mixing is reduced, the supersaturation increases because the seasonal warming is larger, increasing the "potential" supersaturation.[3] If more bubbles are trapped in the winter mixed layer, this adds to the supersaturation produced by *in situ* heating during spring and summer. The effective rate of air injection for argon increases with the fraction of total trapping, since this mode is less limited by boundary-layer diffusion (cf. Jenkins, 1988).

3. The mixing of argon across the seasonal thermocline is also reduced, but the increase in ΔAr_{max} can be accounted for solely by the increase in seasonal warming.

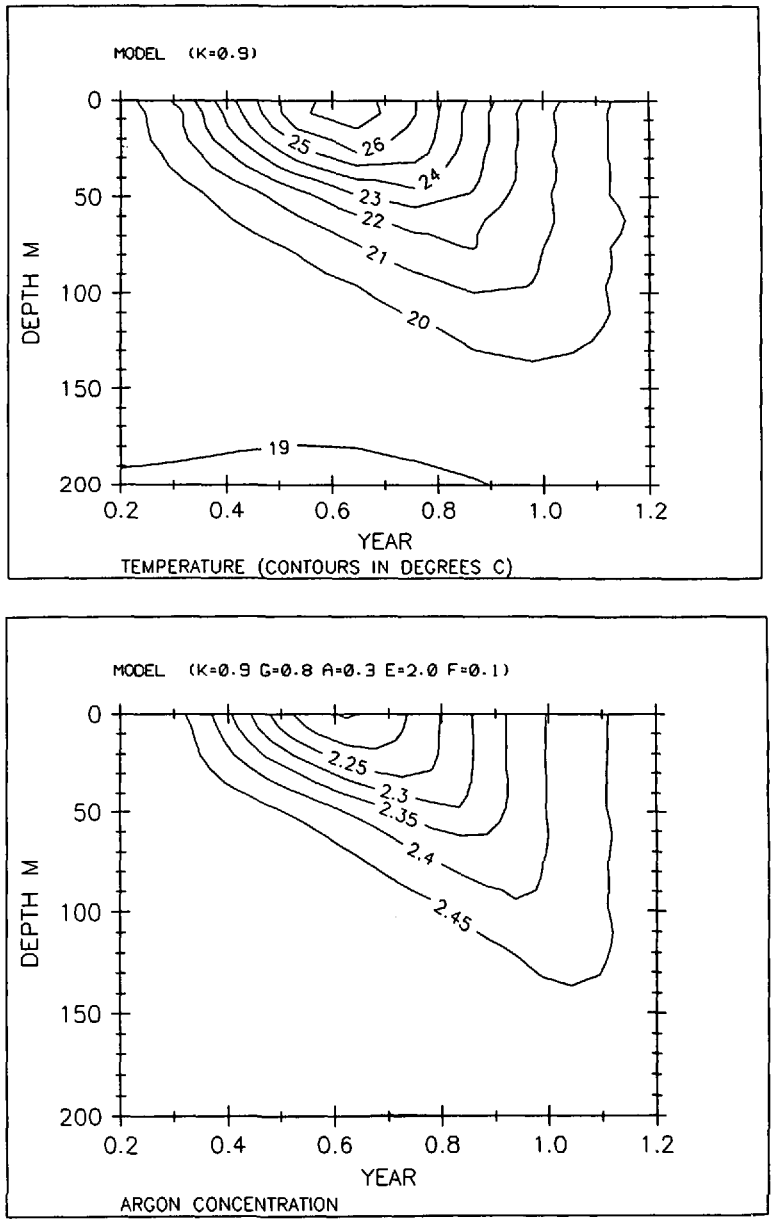

Figure 3. Results of a model run with typical parameters ($\kappa = 0.9$, $g = 0.8$, $a_{inj} = 0.3$, $\gamma = 2.0$, $f_t = 0.1$, $P_{ml} = 6$, $P_{50} = 4$) for (a) temperature (°C), (b) argon concentration (10^{-4} cc g^{-1}), (c) ΔAr (percent supersaturation), and (d) ΔO_2 (percent supersaturation). Units are the same as in Figure 1, but contour intervals differ for ΔAr and ΔO_2. Note that the model simulates the basic features of the data (Fig. 1).

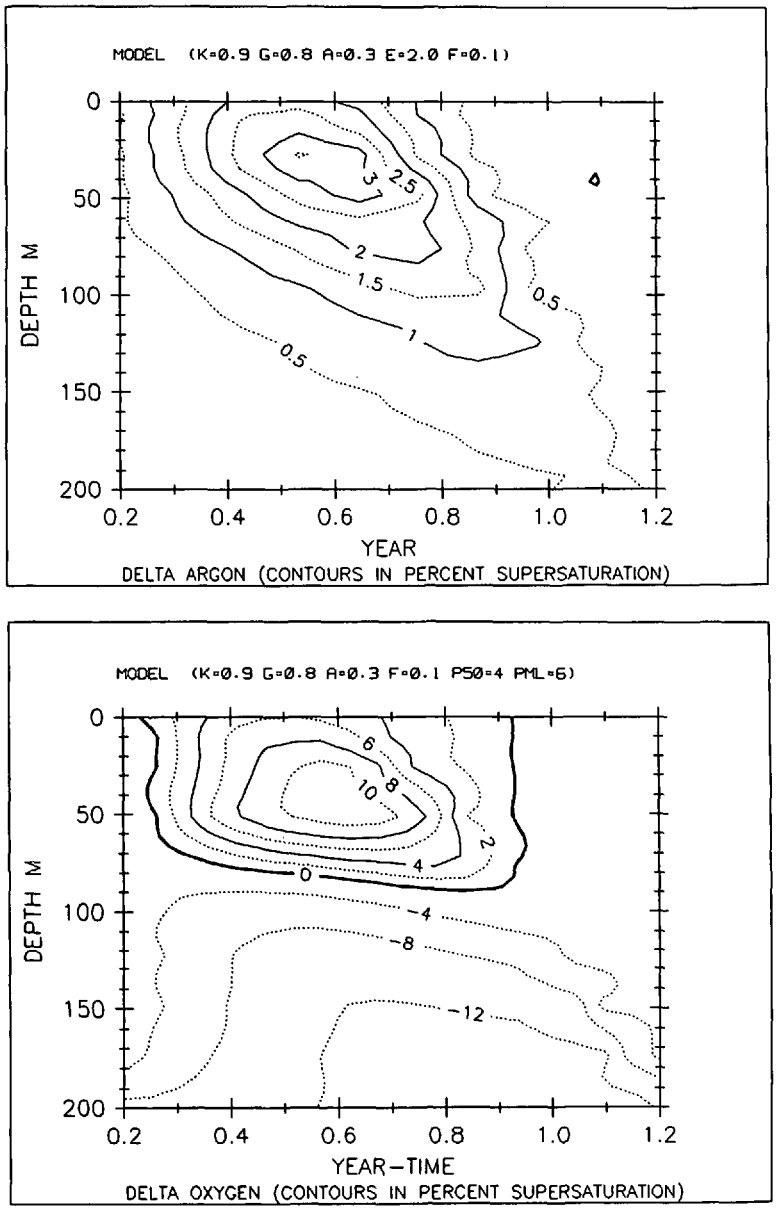

Figure 3. (Continued)

b. Gas exchange and air injection. The degree to which argon approaches solubility equilibrium in the mixed layer depends on the rate of gas exchange, balanced against *in situ* thermal forcing, the rate of air injection, and the flux of argon from below. Since the upward flux of argon into the mixed layer is much smaller than the gas exchange flux, variations in the rate of vertical mixing have little effect. To some extent,

Table 1. For each constraint equation, there is an error associated with linearizing the model response (first column), and an uncertainty associated with measuring features of the tracer distributions (second column), including analytical errors and uncertainty in the solubilities. In most cases, the linearization error is smaller than the measurement error. The total uncertainty for each constraint equation (third column) is calculated as the quadrature sum of the linearization and measurement errors. The final column shows the residuals obtained by comparing the results of the inverse calculation to the data. For each equation, the inversion residual is smaller than the total error associated with that constraint, suggesting that the solution is consistent with all the constraint equations.

Constraint equation	Linearization error	Measurement error	Total error	Inversion residual
(1) $\Delta T_{ml}[s-w]$	0.2°C	0.2°C	0.3°C	0.0°C
(2) $\Delta Ar_{max}[s]$	0.1%	0.4%	0.4%	−0.1%
(3) $\Delta Ar_{ml}[s]$	0.1%	0.4%	0.4%	+0.1%
(4) $\Delta Ar_{ml}[w]$	0.1%	0.3%	0.3%	0.0%
(5) ΔHe_{ml}[mean]	0.1%	0.2%	0.2%	0.0%
(6) $\Delta He_{ml}[w]/\Delta He_{ml}[s]$	0.2	0.1	0.2	0.0
(7) $\Delta O_{2ml}[s-w]$	0.5%	3.0%	3.0%	0.0%
(8) $\Delta O_{2max}[s-w]$	0.2%	3.0%	3.0%	0.0%

increased air injection is indistinguishable from lower gas exchange rates since both increase the mixed layer supersaturations of argon and helium (Fig 5). But, since argon is most sensitive to gas exchange and helium is more sensitive to air injection the two processes can be resolved by using both gases.

As observed in the data, the model predicts that the maximum argon supersatura-

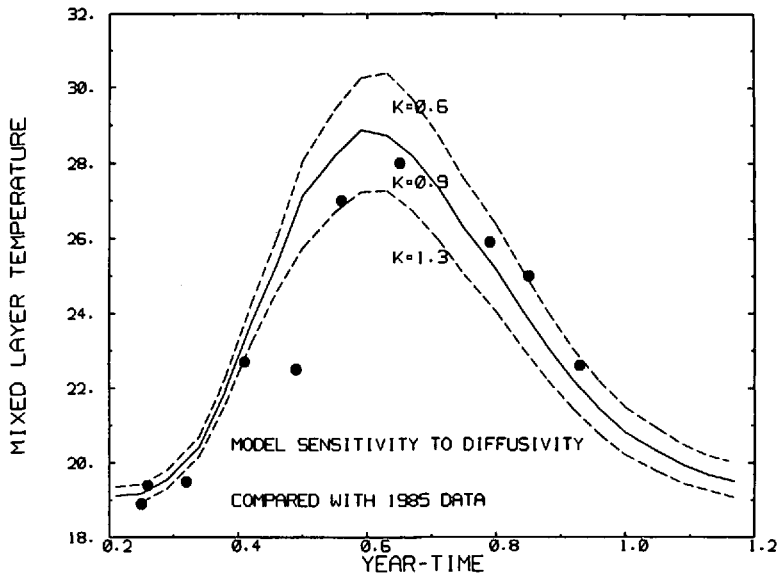

Figure 4. Model sensitivity of mixed layer temperature to κ, compared with 1985 data.

tion in the mixed layer occurs in the summertime. The magnitude of the argon supersaturation in the summer mixed layer ($\Delta Ar_{ml}[s]$) is directly related to the gas exchange rate, and somewhat less sensitive to air injection:

$$\Delta Ar_{ml}[s] = (1/g)\{2.8(a_{inj})(0.2f_t + 0.9) + 1.6\} \pm 0.1\% \quad (3)$$

For a typical model run, air injection contributes about 40% of the summer supersaturation. However, the winter values ($\Delta Ar_{ml}[w]$) are relatively more sensitive to air injection:

$$\Delta Ar_{ml}[w] = (1/g)\{2.9(a_{inj})(1.0f_t + 0.7) - 0.5\} \pm 0.1\% \quad (4)$$

In the absence of air injection, the model predicts that wintertime cooling leads to undersaturation of argon in the mixed layer.

For helium, the average supersaturation in the mixed layer ($\Delta He_{ml}[mean]$) is directly related to the gas exchange rate, but also proportional to air injection:

$$\Delta He_{ml}[mean] = (1/g)(a_{inj})(9.5 - 0.63\gamma) \pm 0.1\% \quad (5)$$

Helium is very sensitive to air injection because of its low solubility, whereas it is relatively insensitive to thermal effects since its solubility has a weak temperature dependence. The model predicts that helium supersaturation is greatest in the winter when air injection is at a maximum, although the data show only a weak seasonal trend (Fig. 2b). The amplitude of seasonal variation of helium supersaturation in the model is directly related to the wind-speed dependence of bubble trapping (γ):

$$\Delta He_{ml}[w]/\Delta He_{ml}[s] = -1.8 + 1.2(\gamma) \pm 0.2 \quad (6)$$

The helium supersaturation in the model is independent of the mode of bubble trapping since we have normalized the total air injection component to that for helium at 20°C. The mixture of partial and complete bubble trapping may vary seasonally, although model runs indicate that this would have a small effect on argon and oxygen supersaturations. Further helium, neon, and argon measurements will address this question.

c. Biological oxygen production. The seasonal distribution of oxygen depends both on physical processes and the rates of new production. In the mixed layer, both model and data show a maximum supersaturation in summertime, when the flux of oxygen from below is only partly compensated by gas exchange loss. The model predicts that the winter mixed layer is slightly undersaturated due to entrainment of oxygen-depleted water from below the euphotic zone, although the data show a small supersaturation near the surface. The seasonal range in percent oxygen supersaturation is determined mainly by the gas exchange rate, air injection and biological production:

$$\Delta O_{2ml}[s - w] = (1/g)(1.8 + 0.7P_{ml} + 0.5P_{50} - 0.8a_{inj}) \pm 0.5\% \quad (7)$$

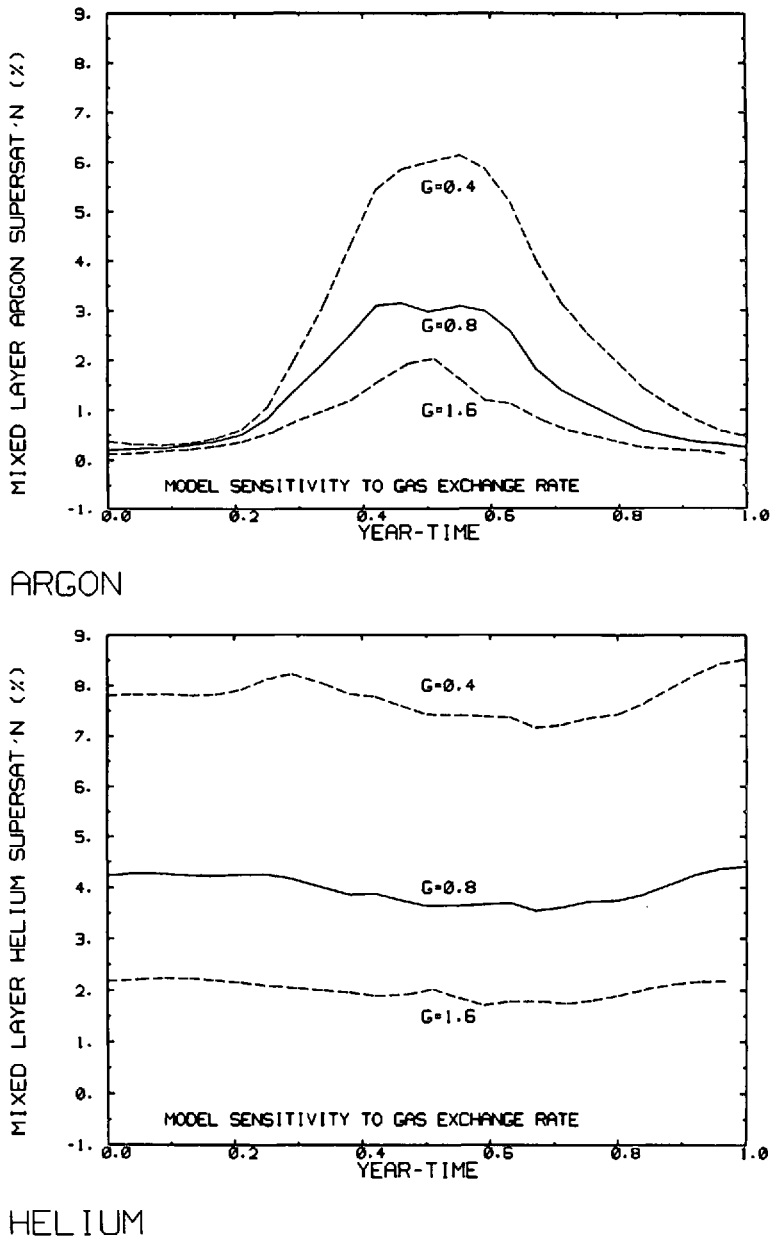

Figure 5. Model sensitivity to variations in gas exchange rate and air injection, using a reference case with $\kappa = 0.9$, $g = 0.8$, $a_{inj} = 0.4$, $\gamma = 2.2$, $f_r = 0.1$. The model predicts that mixed layer distributions of (a) ΔAr and (b) ΔHe are equally sensitive to variations in the gas exchange rate. However, air injection is much less important for (c) ΔAr than for (d) ΔHe.

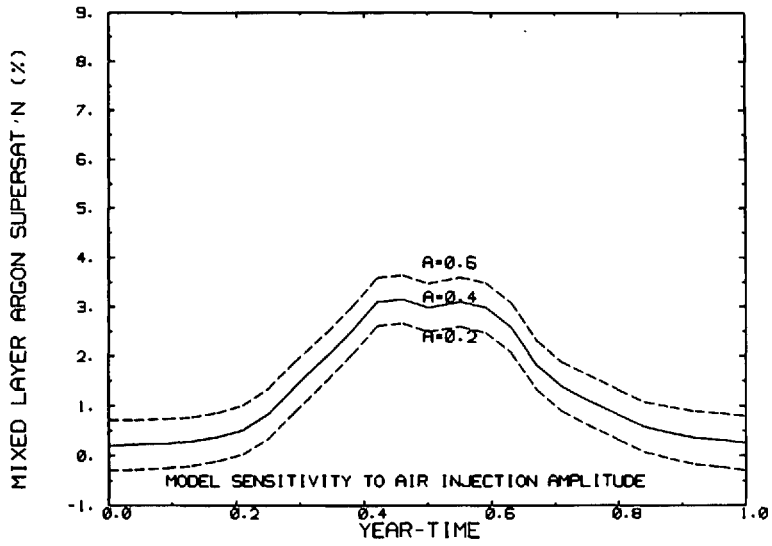

ARGON

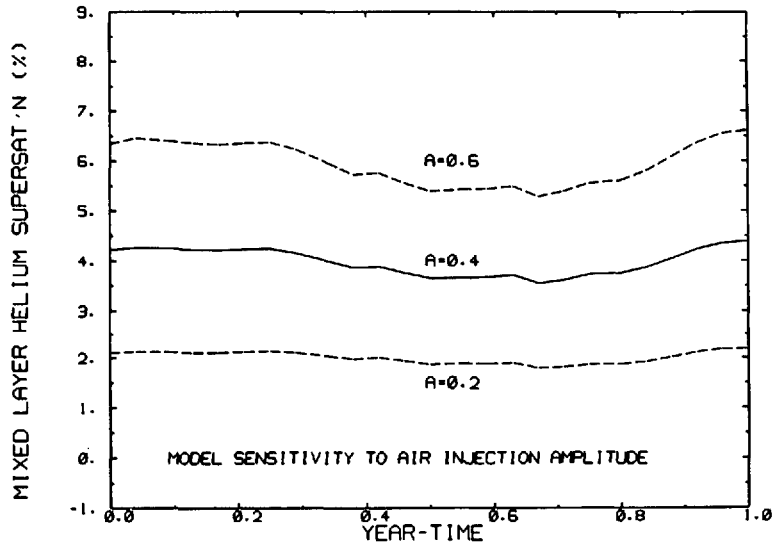

HELIUM

Figure 5. (Continued)

This diagnostic minimizes the effects of air injection, and may minimize the impact of any possible systematic offset in the oxygen data. Although the mixed layer supersaturation increases with mixed layer production, the effect is small. As pointed out by Musgrave *et al.* (1988), this occurs because the gas exchange rate is much faster than the rates of production. Increasing the subsurface production also has an effect, since

this will drive more mixing across the seasonal thermocline. Thus, the mixed layer oxygen data provide only a weak constraint on near-surface oxygen production.

In the seasonal thermocline, the model predicts a summer oxygen maximum similar to that observed in the data. The seasonal range in percent oxygen supersaturation is determined mainly by a balance between subsurface biological production and vertical mixing:

$$\Delta O_{2max}[s - w] = 3.7(10^{-4}/\kappa) + 2.2(1/g) - 0.5(a_{inj}) + 0.2(P_{ml}) + 2.0(P_{50}) - 3.1 \pm 0.2\% \quad (8)$$

As subsurface production is increased, the magnitude of subsurface supersaturation increases. If mixed layer production is large enough it will add to the deeper supersaturation maximum by inhibiting the upward mixing flux.

For oxygen, vertical mixing is more important than for argon since biological production creates larger gradients and hence higher fluxes. Thus the oxygen remaining in the seasonal thermocline may represent only a small fraction of that actually produced by photosynthesis during spring and summer. In this respect argon is not a perfect analog for oxygen, and the model is required to make quantitative inferences.

6. Quantitative estimates

The above relationships form a set of empirically-derived equations that constrain the model parameters in terms of observed temperature and gas cycles. The nonlinear terms in the equations can be approximated with first-order Taylor series expansions, which introduce little additional error over the domain of interest. Since there are more equations (8) than unknowns (7), the resulting system of linear equations is overdetermined. Thus, it is conceivable that there may be no solution that exactly satisfies all the constraints. We chose the solution that best fit the data in a least-squares sense by using the method of singular value decomposition (Press *et al.*, 1986).

First, the relevant indices were extracted from the observations. The temperature record (Fig. 3) in 1985 yielded:

$$\Delta T_{ml}[s - w] = 9.0 \pm 0.2\ ^\circ C$$

To determine the winter and summer values of argon supersaturation, the observed mixed layer averages were fit using a nonlinear least squares technique to a functional form[4] that approximated the model curves (Fig. 2a):

$$\Delta Ar_{ml}[w] = 0.9 \pm 0.2\%$$
$$\Delta Ar_{ml}[s] = 3.0 \pm 0.3\%$$

4. A skewed Gaussian form was used to fit the model curves: $\Delta Ar(t) = \Delta Ar_w + (\Delta Ar_s - \Delta Ar_w) \exp\{-[25 + 10(t - 0.5)](t - 0.5)^2\}$.

Although we have used N.B.S.-traceable argon standards and the best available values for argon solubility, a systematic offset of 0.2–0.3% in the argon supersaturations is possible. But, since the effects of a 0.3% bias in ΔAr are well within the formal uncertainties derived from the inversion we do not consider this an important source of error. The helium supersaturations were fit to sine curves, which approximated the model results. A nonlinear least squares fit yielded (Fig. 2b):

$$\Delta He_{ml}[\text{mean}] = 3.5 \pm 0.3\% \qquad \Delta He_{ml}[\text{ampl}] = 0.2 \pm 0.1\%$$

Thus,

$$\Delta He_{ml}[w]/\Delta He_{ml}[s] = 1.1 \pm 0.1$$

A systematic offset of up to 0.5% in the helium supersaturations is possible (Weiss, 1971b), but again the effects are within the formal uncertainties derived from the inversion. The maximum argon supersaturation in the summer thermocline was derived from Figure 1c:

$$\Delta Ar_{max}[s] = 4.0 \pm 0.3\%$$

The oxygen data in Figure 1d yielded:

$$\Delta O_{2ml}[s - w] = 17 \pm 3\%$$
$$\Delta O_{2max}[s - w] = 14 \pm 3\%$$

using the error estimates derived earlier.

Each equation was weighted by the reciprocal of its estimated uncertainty, derived from estimated measurement errors (including uncertainty in the solubility) and model-linearization errors (Table 1). The solution and estimated uncertainties are:

$$\kappa = 0.91 \pm 0.08 \times 10^{-4}\ \text{m}^2\ \text{s}^{-1}$$
$$a_{\text{inj}} = 0.39 \pm 0.11$$
$$\gamma = 2.2 \pm 0.2$$
$$f_t = 0.07 \pm 0.27$$
$$g = 0.83 \pm 0.12$$
$$P_{ml} = 11.6 \pm 6.7\ \text{moles}\ O_2\ \text{m}^{-2}\ \text{yr}^{-1}$$
$$P_{s0} = 4.3 \pm 1.7\ \text{moles}\ O_2\ \text{m}^{-2}\ \text{yr}^{-1}$$

The residuals are within the estimated errors for each equation (see Table 1), suggesting that the solution is consistent with all constraint equations and that the estimated errors are reasonable.

The sensitivity of the solution to each linearized constraint equation is evident from the weighted matrix of equation coefficients (Table 2). For a given solution parameter, the magnitudes of the coefficients in that column reflect the relative importance of

Table 2. The linearized model constraints form an overdetermined set of simultaneous linear equations. Each equation is weighted by the reciprocal of the total error associated with that equation (see Table 1). The weighted matrix of coefficients in these equations allows a direct comparison of the relative importance of each constraint in determining the solution (see text for details).

	Model parameter						
Constraint eq.	$(1/\kappa)$	(a_{inj})	γ	f_t	$(1/g)$	P_{ml}	P_{50}
(1) $\Delta T_{ml}[s-w]$	9.9	0	0	0	0	0	0
(2) $\Delta Ar_{max}[s]$	2.0	4.4	0	0.8	5.0	0	0
(3) $\Delta Ar_{ml}[s]$	0	6.7	0	0.8	8.0	0	0
(4) $\Delta Ar_{ml}[w]$	0	9.0	0	4.0	3.0	0	0
(5) ΔHe_{ml}[mean]	0	23	0	0	11	0	0
(6) $\Delta He_{ml}[w]/\Delta He_{ml}[s]$	0	0	5.7	0	0	0	0
(7) $\Delta O_{2ml}[s-w]$	0	−0.3	0	0	5.7	0.2	0.1
(8) $\Delta O_{2max}[s-w]$	1.3	−0.2	0	0	0.7	0.06	0.7

each of the constraint equations in determining the value of that parameter. The diffusivity is mainly determined from the mixed layer temperature history, and secondarily by the constraints from the subsurface argon cycle. Air injection amplitude is mainly determined by the mean helium supersaturation, as well as from the mixed layer argon supersaturation. The wind speed dependence of air injection is determined solely by the ratio of winter to summer helium supersaturations. The mixture of partial and total bubble trapping is determined by the relative mixed layer supersaturations of argon and helium, since the total air injection rate is normalized to the latter. The gas exchange rate is determined by the helium and argon supersaturations in the mixed layer. Surface productivity is barely constrained at all, as revealed by the small coefficient terms in this column. The subsurface productivity is determined by the subsurface oxygen data.

7. Discussion

The vertical diffusivity that best matches the observed argon cycle ($0.9 \pm 0.1 \times 10^{-4}$ $m^2 s^{-1}$) is consistent with that required to match the observed 1985 temperature history and similar to the optimal value demanded by the heat budget for the climatological model runs (cf. Musgrave *et al.*, 1988). This estimate is much larger than typical estimates of diapycnal mixing in the *main* thermocline of order 0.1×10^{-4} $m^2 s^{-1}$ (Gargett, 1984; Jenkins, 1980). However, within the *seasonal* thermocline processes other than simple diapycnal diffusion may contribute to the apparent diffusivity. For example, Musgrave *et al.* (1988) have shown that wind-mixing is a significant component.

Our estimate of air injection indicates that this process contributes about 40% of the argon supersaturation observed in the summer mixed layer. The magnitude of this

effect is similar to that predicted by Atkinson (1973) for oxygen at wind speeds of 10 m s^{-1}. Our estimates of the rate of bubble trapping are also of the same order of magnitude as those by Thorpe (1984; 1986) based on single-bubble dynamics applied to bubble populations measured by acoustic scattering. The wind-speed dependence of this rate is similar to the wind-speed dependence of bubble populations estimated by Crawford and Farmer (1987; $\gamma = 3.0 \pm 0.5$) from open ocean acoustic measurements. By combining their estimates of bubble concentrations and size distribution with our estimate of the bubble flux, we estimate a mean bubble lifetime of order 10 seconds. This calculation suggests that the bubble dynamics may be complex, since this lifetime is of the same order as the transit time to the surface, the time for bubble dissolution, and the time-scale for gas exchange between the bubble and bulk seawater (Jahne *et al.*, 1984). Moreover, this rough agreement is consistent with a combination of partial and complete bubble trapping, as inferred from the helium and argon supersaturations. By applying the model described here to GEOSECS measurements of ΔHe and ΔNe, Jenkins (1988) also found that air injection was dominated by partial trapping rather than complete trapping.

The gas exchange rates in 1985 are slightly lower than our best estimate using the Liss and Merlivat (1986) formulation of piston velocity and climatological wind speeds. The agreement is remarkable, considering that the field data are mostly from ^{222}Rn (~5 day timescale) and ^{14}C (~2 year timescale) estimates whereas the argon cycle gives a seasonal average. The discrepancy is within the uncertainty in the wind speeds (±10%) and in the piston velocity vs. wind speed relationship (±15%) (Jenkins, 1988).

Short period variations in wind speed tend to increase the mixed layer supersaturations of helium and argon because the air injection rate has a strongly nonlinear dependence on wind speed. Although the Liss and Merlivat (1986) parameterization of gas exchange rate also has a nonlinear dependence on wind speed, this introduces only a small bias (<5%) in the seasonally averaged gas exchange rate because the changes in slope are relatively small. The wind speed variance in our simulation is within 25% of that obtained by Musgrave *et al.* (1988), who used stochastic winds based on the wind spectrum measured by a meteorological buoy west of Bermuda. The net effect of doubling the amplitude of the short period wind variations is to increase the supersaturations by a factor of 1.1–1.2; halving the amplitude decreases the supersaturations by a factor of 0.90–0.95. Thus, our estimate of gas exchange rate can constrain only the seasonal-average value but not the detailed wind-speed dependence.

The biological production of oxygen is moderately well-determined by the model applied to the data, although near-surface productivity remains unconstrained because the mixed layer concentrations are mainly controlled by gas exchange. The estimate of 4.3 ± 1.7 moles O_2 m^{-2} yr^{-1} for subsurface new production is a lower limit to the depth-integrated production because the surface productivity is unknown. If near-surface productivity is fixed at zero, the inversion predicts a productivity of 5.6 ± 1.5

moles O_2 m^{-2} yr^{-1} and confirms that the former estimate is a lower bound. However, by eliminating near-surface productivity, the inversion residual for the mixed layer oxygen constraint is increased (the model predicts supersaturations smaller than observed). Nevertheless, the latter estimate may be closer to the depth-integrated value since unconstrained near-surface production tends to reduce the required subsurface production in the former estimate.

For the 1985 record, our determination of subsurface production may be limited by the quality of the oxygen data. If the analytical error in the oxygen data were ±0.05 ml l^{-1} subsurface production could be constrained within ±10%. In fact, the 1960–1970 average data are known at this level of precision:

$$\Delta O_{2ml}\,[s - w] = 10.8 \pm 0.6\%$$
$$\Delta O_{2max}\,[s - w] = 11.7 \pm 0.7\%$$

If the oxygen (and temperature) data from this period are combined with the noble gas data from 1985, the inverse calculation yields:

$$\kappa = 1.3 \pm 0.1 \times 10^{-4}\ m^2\ s^{-1}$$
$$P_{ml} = 3.2 \pm 3.2 \text{ moles } O_2\ m^{-2}\ yr^{-1}$$
$$P_{50} = 4.5 \pm 0.4 \text{ moles } O_2\ m^{-2}\ yr^{-1}$$

Clearly, the two data sets are not strictly comparable as seen from the higher diffusivity demanded by the 1960–1970 temperatures; however, this calculation suggests that new production during 1960–1970 was similar to that in 1985 if gas exchange rates for both periods were comparable. In any case, the comparison indicates that better oxygen measurements would constrain the subsurface productivity more tightly, although near-surface productivity would remain unconstrained. New production calculated for the 1960–1970 period matches that calculated by Jenkins and Goldman (1985), while our results for 1985 imply slightly lower productivity despite the fact that oxygen supersaturations in 1985 were slightly larger. This can be attributed to the lower vertical diffusivity determined for 1985. Our estimates of new production are also quite close to those of Musgrave *et al.* (1988), who estimated 3–4 moles O_2 m^{-2} yr^{-1} by applying a similar upper ocean model to the 1960–1970 average data.

Although the model is relatively successful in simulating the seasonal temperature and gas cycles, it ignores lateral transport. Above the depth of winter convection (typically 150–200 m), local surface forcing will tend to control the temperature and gas distributions. However, lateral (e.g. isopycnal) processes are undoubtedly important in ventilating the underlying density surfaces (Jenkins, 1980). These effects are probably less significant for temperature and argon than for nonconservative tracers such as nitrate and ^3He which may have larger isopycnal gradients. Oxygen will tend to be intermediate because it is controlled both by the temperature dependence of its

solubility and by biological production. Isopycnal mixing will tend to reduce the size of subsurface anomalies. Since we have not accounted for isopycnal mixing, we may be underestimating the magnitude of the oxygen excess produced in the seasonal thermocline. Thus, we may be underestimating the biological oxygen production required.

In fact, lateral effects may explain some of the differences between the 1985 data and the composite seasonal cycle discussed by Jenkins and Goldman (1985). Although the basic features are similar, the subsurface oxygen maximum in 1985 is substantially larger than in the average record and persists well into the fall, during which the upper 200 m were also much warmer than average. Although the oxygen and temperature cycles in 1985 are well within the ranges observed for individual years in the historical record at Station S, the one-year record appears "noisier." This is not surprising because the longer record will tend to smooth out irregularities due to passage of advected features (e.g. mesoscale eddies) and interannual variations in meteorological forcing (e.g. wind stress, air-sea heat flux).

8. Summary

The seasonal cycle of argon near Bermuda demonstrates unequivocally that only a small fraction of the subsurface oxygen supersaturation maximum can be attributed to physical causes, and therefore that most of the supersaturation must be attributed to photosynthetic oxygen production. Furthermore, the evolution of argon concentration in the seasonal thermocline suggests that most of the oxygen produced there is also lost due to vertical mixing and gas exchange. The subsurface evolution of argon concentration requires a vertical diffusivity of $0.9 \pm 0.1 \times 10^{-4}$ m^2 s^{-1}, consistent with that derived from temperature. Measurements of argon and helium supersaturation determine the rate of air injection to ±25% and the seasonally-averaged gas exchange rate to ±12%. The inferred rate of bubble trapping is roughly consistent with previous work by Atkinson (1973), Thorpe (1984; 1986), and Crawford and Farmer (1987), and this process is dominated by partial trapping as suggested by Jenkins (1988). Our estimate of gas exchange rate is 17% lower than that predicted from climatological wind speeds and Liss and Merlivat's (1986) formulation of piston velocity. A lower limit to new production of oxygen is estimated as 4.3 ± 1.7 moles m^{-2} yr^{-1}, and the uncertainty in the estimate might be reduced with higher quality oxygen data. If the near-surface new production is fixed at zero, we estimate 5.6 ± 1.5 moles O_2 m^{-2} yr^{-1}. Our estimate is close to the results obtained by Jenkins and Goldman (1985) and Musgrave *et al.* (1988) for the 1960–1970 period.

Acknowledgments. This work would be impossible without the dedicated efforts of Tim Jickells and Rachael Sheriff-Dow at the Bermuda Biological Station and the seamanship of Captain Michael Rhodes and Engineer Tony Sheriff of the R/V *Weatherbird*. The staff of the WHOI Helium Isotope Laboratory, especially Dempsey Lott and Marcia Davis, has provided

invaluable support and guidance. Discussions with Scott Doney, Dave Musgrave, and Dave Glover were also helpful. This project is supported by NSF grant OCE85-01171. Contribution no. 6799 from the Woods Hole Oceanographic Institution.

APPENDIX

Station S argon data April 1985–April 1986

Sta. no.	Year* time	Bt** no.	Depth (m)	Temp. (°C)	Salt (‰)	Ar Conc.*** 10^{-4}cc g^{-1}	ΔAr† (%)	ΔHe† (%)	ΔO_2† (%)
562	85.25	27	1	19.04	36.521	2.494	0.3	—	4.8
562	85.25	1	1	19.07	36.530	2.541	2.3	3.1	4.8
562	85.25	2	10	18.86	36.526	—	—	4.3	4.4
562	85.25	28	10	18.86	36.520	2.513	0.7	0.0	5.6
562	85.25	29	20	18.72	36.520	2.546	1.8	—	4.9
562	85.25	3	25	18.79	36.522	2.505	0.3	3.8	4.3
562	85.25	30	30	18.86	36.525	2.538	1.7	—	4.0
562	85.25	31	41	18.70	36.524	2.528	1.0	—	2.0
562	85.25	4	50	18.82	36.514	2.572	3.0	3.8	2.2
562	85.25	33	60	18.69	36.516	2.550	1.9	3.9	−0.7
562	85.25	34	70	18.65	36.511	2.512	0.3	—	0.7
562	85.25	35	80	18.65	36.511	2.508	0.1	—	0.7
562	85.25	36	91	18.62	36.522	—	—	3.6	0.7
562	85.25	37	125	18.64	36.522	2.511	0.2	8.7	0.7
562	85.25	38A	173	18.61	36.521	2.503	−0.2	4.7	0.3
562	85.25	38B	173	18.61	36.521	2.536	1.1	—	0.3
562	85.25	8	190	18.64	36.519	2.516	0.3	5.1	0.7
562	85.25	9	239	18.59	36.529	2.517	0.3	2.7	0.6
562	85.25	10	288	18.60	36.520	2.533	1.0	—	0.6
562	85.25	11	336	18.16	36.460	2.571	1.6	—	−9.0
562	85.25	12A	386	18.03	36.454	2.487	−2.0	5.2	−11.5
562	85.25	12B	386	18.03	36.454	2.557	0.7	—	−11.5
562	85.25	24	2188	3.60	34.977	3.484	−0.2	7.3	−15.3
564	85.32	27	1	20.33	36.479	2.514	3.5	—	5.7
564	85.32	1	1	19.95	36.488	—	—	5.7	6.7
564	85.32	28	5	19.51	36.468	2.532	2.7	3.7	5.7
564	85.32	2	10	19.46	36.486	—	—	5.8	6.5
564	85.32	30	31	19.40	36.482	—	—	4.8	4.5
564	85.32	3	25	19.43	36.479	2.541	2.9	—	6.5
564	85.32	31	43	19.20	36.487	2.512	1.3	—	5.1
564	85.32	32	52	18.99	36.525	—	—	5.5	3.7
564	85.32	33	61	18.88	36.526	2.544	2.0	4.9	3.3
564	85.32	34	68	18.81	36.534	2.514	0.7	4.3	0.1
564	85.32	35	78	18.74	36.536	—	—	4.6	−1.0
564	85.32	36	89	18.82	36.531	2.548	2.0	5.4	−0.5
564	85.32	37	127	18.57	36.521	2.534	1.0	5.7	−1.1
564	85.32	38A	167	18.46	36.50	2.553	1.6	—	−3.4
564	85.32	38B	167	18.46	36.50	2.572	2.3	—	−3.4
566	85.41	1	1	22.80	36.397	—	—	5.7	7.2

APPENDIX

Sta. no.	Year* time	Bt** no.	Depth (m)	Temp. (°C)	Salt (‰)	Ar Conc.*** 10^{-4}cc g^{-1}	ΔAr† (%)	ΔHe† (%)	ΔO_2† (%)
566	85.41	27	1	22.97	36.407	2.405	3.6	4.5	5.6
566	85.41	28	5	22.37	36.392	2.394	2.0	4.6	4.5
566	85.41	29	10	22.06	36.413	2.411	2.3	3.5	7.4
566	85.41	2	10	22.04	36.415	2.420	2.6	3.3	7.8
566	85.41	25	25	21.69	36.422	—	—	4.0	5.3
566	85.41	30	20	21.95	36.417	2.404	1.7	3.2	8.4
566	85.41	31	30	21.20	36.441	—	—	4.7	8.4
566	85.41	32	40	20.45	36.473	2.468	1.8	3.6	7.7
566	85.41	33	50	19.78	36.508	2.522	2.8	4.4	9.1
566	85.41	34	60	19.24	36.493	2.512	1.3	7.0	9.2
566	85.41	35	70	18.82	36.486	2.521	0.9	4.8	1.2
566	85.41	36	81	19.02	36.491	2.525	1.4	4.6	4.7
566	85.41	37	91	18.61	36.494	2.503	−0.2	5.1	−1.3
566	85.41	38	127	18.37	36.483	—	—	6.3	−0.2
566	85.41	39	176	18.23	36.505	2.554	1.1	6.0	−1.4
567	85.49	1	1	26.13	36.516	2.308	4.8	4.9	9.2
567	85.49	1	1	26.25	36.496	—	—	3.5	11.8
567	85.49	28	5	25.73	36.485	2.265	2.2	4.3	6.9
567	85.49	29	9	25.66	36.478	2.294	3.4	4.1	8.3
567	85.49	30	18	23.96	36.543	2.353	3.2	—	9.6
567	85.49	31	26	22.04	36.583	—	—	4.9	9.9
567	85.49	32	33	21.39	36.569	2.476	3.9	7.3	7.6
567	85.49	33	40	20.69	36.546	2.487	3.0	2.2	9.8
567	85.49	34	46	20.31	36.543	2.526	4.0	5.8	6.7
567	85.49	35	55	19.92	36.538	2.529	3.3	4.5	7.8
567	85.49	36	66	19.91	36.536	2.504	2.3	4.0	4.7
567	85.49	37	76	19.32	36.543	2.507	1.3	—	1.8
567	85.49	39A	179	18.50	36.568	2.517	0.2	6.2	−5.8
567	85.49	39B	179	18.50	36.568	2.561	1.9	4.2	−5.8
567	85.49	24	2156	3.61	34.972	3.449	−1.2	7.5	−18.3
569	85.56	27	1	27.25	36.436	2.229	3.1	—	24.0
569	85.56	1	1	27.05	36.439	—	—	3.9	26.5
569	85.56	28	5	26.94	36.435	2.227	2.5	—	17.2
569	85.56	2	10	26.48	36.415	—	—	6.2	24.0
569	85.56	29	10	26.65	36.434	2.224	1.8	3.0	12.9
569	85.56	3	24	26.29	36.415	—	—	3.8	16.0
569	85.56	30	20	26.47	36.466	2.303	5.1	3.0	19.0
569	85.56	31	30	25.59	36.378	2.292	3.1	—	15.9
569	85.56	32	39	22.11	36.562	2.478	5.2	—	18.7
569	85.56	33	49	21.06	36.602	2.474	3.2	3.8	15.1
569	85.56	34	59	20.87	36.543	2.500	3.9	4.8	14.7
569	85.56	35	68	20.06	36.545	2.488	1.9	—	16.7
569	85.56	36	77	19.56	36.528	2.501	1.5	3.1	11.2

APPENDIX

Sta. no.	Year* time	Bt** no.	Depth (m)	Temp. (°C)	Salt (‰)	Ar Conc.*** 10^{-4}cc g^{-1}	ΔAr† (%)	ΔHe† (%)	ΔO_2† (%)
569	85.56	37	87	19.35	36.541	—	—	4.2	0.5
569	85.56	38	119	18.90	36.523	2.502	0.3	—	1.8
569	85.56	39	177	18.59	36.564	2.523	0.6	3.5	0.4
569	85.56	24	2152	3.61	34.986	3.452	−1.1	6.4	−14.5
571	85.65	1	1	28.31	36.461	2.227	4.7	4.0	26.0
571	85.65	27	1	28.70	36.470	—	—	6.7	16.4
571	85.65	28	5	27.62	36.468	2.189	1.9	0.2	18.1
571	85.65	29	8	27.46	36.459	2.210	2.5	3.4	11.4
571	85.65	2	10	27.41	36.446	2.188	1.4	3.0	20.1
571	85.65	30	13	27.53	36.529	2.204	2.4	5.6	19.5
571	85.65	31	21	27.34	36.451	—	—	3.7	16.5
571	85.65	3	24	27.25	36.463	2.192	1.4	2.4	18.7
571	85.65	32	30	26.37	36.490	2.242	2.3	4.4	17.7
571	85.65	33	39	22.88	36.549	2.451	5.5	2.9	21.0
571	85.65	34	48	21.67	36.562	2.467	4.0	3.0	16.0
571	85.65	35	67	20.42	36.544	2.478	2.2	4.7	13.4
571	85.65	5	68	19.80	36.527	2.499	1.9	3.2	13.2
571	85.65	37	86	19.47	36.528	2.498	1.2	3.2	6.9
571	85.65	6	92	19.16	36.512	2.504	0.9	6.6	−0.4
571	85.65	38	121	18.92	36.519	2.500	0.3	3.6	0.3
571	85.65	39	182	18.41	36.555	2.518	0.1	5.8	1.6
571	85.65	24	2174	3.61	34.984	3.486	−0.1	—	−15.6
571	85.65	25	2369	3.63	34.972	3.473	−0.5	7.5	−11.4
574	85.79	27	1	25.98	36.358	2.260	2.3	10.4	13.1
574	85.79	1	1	25.95	36.360	—	—	3.2	16.8
574	85.79	28	5	25.68	36.358	2.272	2.3	3.8	17.5
574	85.79	2	10	25.64	36.356	—	—	3.4	12.7
574	85.79	29	10	25.69	36.357	2.256	1.7	5.0	12.6
574	85.79	30	20	25.71	36.398	2.253	1.6	6.2	11.1
574	85.79	3	25	25.79	36.369	—	—	2.8	15.4
574	85.79	32	48	25.65	36.352	2.252	1.4	2.6	9.1
574	85.79	33	51	25.64	36.361	2.232	0.5	4.4	12.7
574	85.79	4	54	25.67	36.358	—	—	2.8	16.2
574	85.79	35	69	25.11	36.377	2.257	0.7	3.3	11.9
574	85.79	5	77	25.12	36.389	—	—	4.0	11.5
574	85.79	36	80	24.1	36.554	2.327	2.1	—	9.4
574	85.79	37	88	23.28	36.597	2.345	1.6	—	4.2
574	85.79	38	123	21.66	36.660	2.402	1.3	2.4	−1.3
574	85.79	39A	165	19.63	36.668	2.474	0.6	5.3	−5.5
574	85.79	39B	165	19.63	36.668	2.474	0.6	6.1	−5.5
574	85.79	24	2211	3.80	34.986	3.468	−0.2	5.5	−13.0
577	85.85	27	3	25.04	36.504	2.280	1.7	5.5	7.4
577	85.85	28	5	24.92	36.411	2.261	0.6	—	5.4

APPENDIX

Sta. no.	Year* time	Bt** no.	Depth (m)	Temp. (°C)	Salt (‰)	Ar Conc.*** 10^{-4}cc g^{-1}	ΔAr† (%)	ΔHe† (%)	ΔO_2† (%)
577	85.85	2	10	24.87	36.668	—	—	1.9	3.8
577	85.85	29	10	24.89	36.413	2.330	3.6	3.9	—
577	85.85	30	21	24.93	36.446	—	—	2.2	−3.3
577	85.58	3	25	24.95	36.546	—	—	1.9	9.0
577	85.85	31	31	24.89	36.417	—	—	1.8	3.9
577	85.85	32	42	24.89	36.418	2.246	−0.1	2.7	6.4
577	85.85	4	52	24.90	36.429	—	—	2.5	8.8
577	85.85	33	53	24.89	36.420	2.275	1.2	—	5.4
577	85.85	34	63	24.90	36.410	2.244	−0.2	3.8	4.5
577	85.85	35	74	24.88	36.414	2.242	−0.3	2.5	1.9
577	85.85	5	79	24.86	36.518	—	—	3.9	6.4
577	85.85	36	84	24.89	36.418	—	—	4.0	8.8
577	85.85	37	94	24.77	36.418	2.257	0.2	2.1	−14.4
577	85.85	6	108	24.77	36.594	—	—	2.8	8.6
577	85.85	38	129	24.70	36.516	—	—	3.9	1.4
577	85.85	39	182	21.39	36.637	—	—	5.0	−4.4
577	85.85	24	2222	3.56	34.826	3.441	−1.7	—	−16.7
580	85.93	1	1	22.74	36.570	—	—	3.1	7.6
580	85.93	27	1	22.83	36.563	2.346	0.9	—	14.9
580	85.93	28	5	22.80	36.559	—	—	2.7	17.1
580	85.93	29	10	22.78	36.628	2.336	0.4	—	4.2
580	85.93	2	11	22.74	36.555	—	—	2.9	13.5
580	85.93	30	21	22.28	36.558	—	—	3.4	4.4
580	85.93	3	26	22.84	36.589	—	—	1.4	18.5
580	85.93	31	32	22.78	36.577	2.334	0.3	—	17.1
580	85.93	32	42	22.74	36.564	2.334	0.2	—	10.0
580	85.93	4	53	22.64	36.551	—	—	1.7	15.5
580	85.93	33	55	22.73	36.559	2.348	0.8	2.9	6.5
580	85.93	34	69	22.71	36.556	2.377	2.0	—	8.7
580	85.93	35	72	22.65	36.558	2.335	0.1	2.0	13.3
580	85.93	36	83	22.64	36.567	—	—	9.0	8.6
580	85.93	37	91	22.63	36.558	2.334	0.0	6.3	11.0
580	85.93	38	127	21.44	36.659	2.414	1.4	3.0	−3.9
580	85.93	7	161	19.93	36.586	—	—	3.5	−1.1
580	85.93	39	173	19.69	36.687	2.498	1.7	2.4	−5.8
580	85.93	24	2222	3.50	34.990	3.466	−1.0	5.4	−9.7
584	86.09	27	1	20.29	36.537	2.432	0.0	2.4	16.5
584	86.09	28	5	20.28	36.559	2.424	−0.3	—	14.1
584	86.09	29	10	20.26	36.561	2.431	−0.1	2.8	15.8
584	86.09	30	20	20.27	36.569	2.419	−0.5	3.1	13.5
584	86.09	3	25	23.93	36.568	—	—	4.4	12.3
584	86.09	31	31	20.38	36.560	2.443	0.6	3.1	14.7
584	86.09	32	41	20.23	36.554	2.427	−0.3	3.5	20.8

APPENDIX

Sta. no.	Year* time	Bt** no.	Depth (m)	Temp. (°C)	Salt (‰)	Ar Conc.*** 10^{-4}cc g^{-1}	ΔAr† (%)	ΔHe† (%)	ΔO_2† (%)
584	86.09	33	52	20.25	36.563	2.414	−0.8	6.0	12.8
584	86.09	34	63	20.22	36.608	2.428	−0.2	3.8	17.7
584	86.09	5	74	20.10	36.543	—	—	4.5	12.5
584	86.09	35	74	20.26	36.555	2.435	0.1	3.9	16.4
584	86.09	36	84	20.13	36.552	—	—	3.3	12.6
584	86.09	37	95	19.76	36.557	2.474	0.8	6.1	6.9
584	86.09	6	98	18.82	36.554	—	—	3.7	1.3
584	86.09	38	131	19.16	36.561	2.491	0.4	3.8	5.2
584	86.09	39A	174	18.52	36.541	2.510	−0.1	6.0	4.8
584	86.09	39B	174	18.52	36.541	2.513	0.0	—	4.8
585	86.26	27	1	—	36.459	2.463	—	—	—
585	86.26	28	5	19.87	36.454	2.474	0.9	3.3	−4.6
585	86.26	2	10	19.72	36.448	—	—	2.6	14.0
585	86.26	29	10	19.81	36.453	2.489	1.5	3.4	4.3
585	86.26	30	20	19.64	36.447	2.470	0.4	2.4	7.4
585	86.26	31	31	19.64	36.461	2.557	3.9	3.9	5.3
585	86.26	33	51	19.42	36.473	2.496	1.0	2.7	−0.9
585	86.26	34	68	19.44	36.486	2.484	0.6	3.4	4.9
585	86.26	35	71	19.44	36.508	2.480	0.4	2.5	6.9
585	86.26	5	79	19.28	36.543	—	—	3.5	2.0
585	86.26	36	81	19.28	36.552	—	—	5.1	12.8
585	86.26	37	91	19.27	36.568	2.472	−0.2	7.6	12.7
585	86.26	6	101	19.22	36.538	—	—	3.2	10.7
585	86.26	38	125	19.19	36.561	2.560	3.2	—	10.8
585	86.26	7	151	19.13	36.537	—	—	2.8	6.4
585	86.26	39A	177	19.07	36.598	2.511	1.0	—	3.7
585	86.26	39B	177	19.07	36.598	2.482	−0.1	—	3.7
585	86.26	8	203	18.83	36.525	—	—	3.2	4.7
585	86.26	26	2467	3.31	34.983	3.479	−1.1	2.9	−17.6

*Year-time is computed as the fraction of the year elapsed since January 1 (e.g. 85.50 is equivalent to July 1, 1985).

**Labels A and B refer to samples drawn consecutively from a single Niskin bottle.

***Argon concentrations are measured in units of 10^{-4} (cc @ S.T.P.) (g seawater)$^{-1}$.

†Saturation anomalies are expressed in percent deviation from solubility equilibrium at the potential temperature and salinity of the sample.

REFERENCES

Atkinson, L. P. 1973. The effect of air bubble solution on air-sea exchange. J. Geophys. Res., *78*, 962–968.

Benson, B. B. 1965. Some thoughts on gases dissolved in the oceans, *in* Proc. Symp. on Mar. Geochem. D. R. Schink and J. T. Corless, eds., Univ. of Rhode Island Occasional Publ. No. 3, 91–107.

Bunker, A. F. 1975. Energy exchange at the surface of the western North Atlantic Ocean. W.H.O.I. Tech. Report 75–3, 107 pp.

Carritt, D. E. and J. H. Carpenter. 1966. Comparison and evaluation of currently employed modifications of the Winkler Method for determining dissolved oxygen in seawater; NASCO report. J. Mar. Res., *24,* 286–318.

Chou, J. Z. 1985. Numerical modelling of oxygen cycling in the upper ocean. W.H.O.I. S.S.F. Report No. 42 (unpublished), 50 pp.

Craig, H. and T. Hayward. 1987. Oxygen supersaturations in the ocean: biological vs. physical contributions. Science, *235,* 199–202.

Crawford, G. B. and D. M. Farmer. 1987. On the spatial distribution of ocean bubbles. J. Geophys. Res., *92,* 8231–8243.

Gargett, A. E. 1984. Vertical eddy diffusivity in the ocean interior. J. Mar. Res., *42,* 359–393.

Isemer, H. J. and L. Hasse. 1985. The Bunker Climate Atlas of the North Atlantic Ocean, Springer-Verlag, Berlin, 218 pp.

Jahne, B., T. Wais and M. Barabas. 1984. A new optical bubble measuring device: a simple model for bubble contribution to gas exchange, *in* Gas Transfer at Water Surfaces, W. Brutsaert and G. H. Jirka, eds., Reidel Publ. Co., 237–246.

Jenkins, W. J. 1980. Tritium and ^{3}He in the Sargasso Sea. J. Mar. Res., *38,* 533–569.

—— 1987. ^{3}H and ^{3}He in the Beta Triangle: observations of gyre ventilation and oxygen utilization rates. J. Phys. Oceanogr., *17,* 763–783.

—— 1988. Using anthropogenic tritium and ^{3}He to study subtropical gyre ventilation and circulation. Phil. Trans. Roy. Soc. London, *A325,* 43–61.

Jenkins, W. J. and W. B. Clarke. 1976. The distribution of ^{3}He in the western Atlantic Ocean. Deep Sea Res., *23,* 481–494.

Jenkins, W. J. and J. C. Goldman. 1985. Seasonal oxygen cycling and primary production in the Sargasso Sea. J. Mar. Res., *43,* 465–491.

Leetmaa, A. and A. F. Bunker. 1978. Updated charts of the mean annual wind stress, convergences in the Ekman layers and Sverdrup transports in the North Atlantic. J. Mar. Res., *36,* 311–322.

Liss, P. S. and L. Merlivat. 1986. Air-sea gas exchange rates: introduction and synthesis, *in* The Role of Air-Sea Exchange in Geochemical Cycling, P. Buat-Menard, ed., Reidel Publ. Co., 113–127.

Lott, D. E. and W. J. Jenkins. 1984. An automated cryogenic charcoal trap system for helium isotope mass spectrometry. Rev. Sci. Instrum., *55,* 1982–1988.

Musgrave, D. L., J. Chou and W. J. Jenkins. 1988. Application of a model of upper ocean physics for studying seasonal cycles of oxygen. J. Geophys. Res. (in press).

Paulson, C. A. and J. J. Simpson. 1977. Irradiance measurements in the upper ocean. J. Phys. Oceanogr., *7,* 952–956.

Press, W. H., B. P. Flannery, S. A. Teukolsky and W. T. Vetterling. 1986. Numerical Recipes, Cambridge University Press, NY 818, pp.

Price, J. F., R. A. Weller and R. Pinkel. 1986. Diurnal cycling: observations and models of upper ocean response to diurnal heating, cooling and wind mixing. J. Geophys. Res., *91,* 8411–8427.

Schulenberger, E. and J. L. Reid. 1981. The Pacific shallow oxygen maximum, deep chlorophyll maximum and primary productivity, reconsidered. Deep-Sea Res., *28,* 901–919.

Spitzer, W. S. and W. J. Jenkins. 1986. Argon as an abiogenic analog of oxygen in upper ocean seasonal gas cycles. EOS Trans. Amer. Geophys. Union, *67,* 1018.

—— 1987. The seasonal cycle of argon in the upper Sargasso Sea. EOS Trans. Amer. Geophys. Union, *68,* 1700.

Thorpe, S. A. 1984. The role of bubble produced by breaking waves in supersaturating the near-surface ocean mixing layer with oxygen. Annales Geophysicae, *2,* 53–56.
—— 1986. Measurements with an automatically recording inverted echo sounder; ARIES and the bubble clouds. J. Phys. Oceanogr., *16,* 1462–1478.
Weiss, R. F. 1968. Piggyback sampler for dissolved gas studies on sealed water samples. Deep-Sea Res., *15,* 695–699.
—— 1970. The solubility of nitrogen, oxygen and argon in water and seawater. Deep-Sea Res., *17,* 721–735.
—— 1971a. The effect of salinity on the solubility of argon in seawater. Deep-Sea Res., *18,* 225–230.
—— 1971b. The solubility of helium and neon in water and seawater. J. Chem. Eng. Data, *16,* 235–241.

Received: *18 May, 1988;* revised: *3 October, 1988.*